GA–A24052

RECENT EXPERIMENTAL STUDIES OF EDGE AND INTERNAL TRANSPORT BARRIERS IN THE DIII–D TOKAMAK

by
P. GOHIL, L.R. BAYLOR, K.H. BURRELL, T.A. CASPER, E.J. DOYLE,
C.M. GREENFIELD, T.C. JERNIGAN, J.E. KINSEY, C.J. LASNIER,
R.A. MOYER, M. MURAKAMI, T.L. RHODES, D.L. RUDAKOV,
G.M. STAEBLER, G. WANG, J.G. WATKINS, W.P. WEST, and L. ZENG

AUGUST 2002

DISCLAIMER

GA–A24052

RECENT EXPERIMENTAL STUDIES OF EDGE AND INTERNAL TRANSPORT BARRIERS IN THE DIII–D TOKAMAK

by
P. GOHIL, L.R. BAYLOR,* K.H. BURRELL, T.A. CASPER,† E.J. DOYLE,‡
C.M. GREENFIELD, T.C. JERNIGAN,* J.E. KINSEY,¶ C.J. LASNIER,†
R.A. MOYER,Δ M. MURAKAMI,* T.L. RHODES,‡ D.L. RUDAKOV,Δ
G.M. STAEBLER, G. WANG,‡ J.G. WATKINS,∞ W.P. WEST, and L. ZENG‡

This is a preprint of an invited paper to be presented at the International Congress on Plasma Physics, July 15-19, 2002, Sydney, Australia, and to be published in the *Proceedings*.

*Oak Ridge National Laboratory, Oak Ridge, Tennessee.
†Lawrence Livermore National Laboratory, Livermore, California.
‡University of California, Los Angeles, California.
¶Lehigh University, Bethlehem, Pennsylvania.
ΔUniversity of California, San Diego, California.
∞Sandia National Laboratories, Albuquerque, New Mexico.

Work supported by
the U.S. Department of Energy under
Contract Nos. DE-AC03-99ER54463, DE-AC05-00OR22725,
W-7405-ENG-48, DE-FG03-01ER54615, DE-FG02-92ER54141,
DE-FG03-95ER54294, and DE-AC04-94AL85000

GENERAL ATOMICS PROJECT 30033
AUGUST 2002

Abstract

Results from recent experiments on the DIII-D tokamak have revealed many important details on transport barriers at the plasma edge and in the plasma core. These experiments include: (a) the formation of the H-mode edge barrier directly by pellet injection; (b) the formation of a quiescent H-mode edge barrier (QH-mode) which is free from edge localized modes (ELMs), but which still exhibits good density and radiative power control; (c) the formation of multiple transport barriers, such as the quiescent double barrier (QDB) which combines a internal transport barrier with the quiescent H-mode edge barrier. Results from the pellet-induced H-mode experiments indicate that: (a) the edge temperature (electron or ion) is not a critical parameter for the formation of the H-mode barrier, (b) pellet injection leads to an increased gradient in the radial electric field, E_r, at the plasma edge; (c) the experimentally determined edge parameters at barrier transition are well below the predictions of several theories on the formation of the H-mode barrier, (d) pellet injection can lower the threshold power required to form the H-mode barrier. The quiescent H-mode barrier exhibits good density control as the result of continuous magnetohydrodynamic (MHD) activity at the plasma edge called the edge harmonic oscillation (EHO). The EHO enhances the edge particle transport whilst maintaining a good energy transport barrier. The ability to produce multiple barriers in the QDB regime has led to long duration, high performance plasmas with $\beta_{NH_{89}}$ values of 7 for up to 10 times the confinement time. Density profile control in the plasma core of QDB plasmas has been demonstrated using on-axis ECH.

1 Introduction

The attainment of steady-state, high-performance fusion plasmas requires control of energy and particle transport in these plasmas. The reduction of cross-field transport through barriers at the plasma edge and/or in the plasma interior is important in advancing the performance capability of tokamaks. Increased understanding of transport barrier physics has resulted from determining the mechanisms which can stabilize plasma turbulence and, thereby, reduce turbulence-driven transport. Leading mechanisms for turbulence stabilization include: (a) reduction of plasma turbulence by E×B velocity shear nonlinear decorrelation of turbulence [1, 2] or by E×B stabilization of turbulent modes [3, 4]; and (b) reduction of the turbulent growth rates by the Shafranov shift (α-stabilization) [5, 6] in the presence of low or negative magnetic shear, which in itself stabilizes high-n MHD modes (e.g., ballooning modes). In the DIII-D tokamak, a long succession of detailed measurements of kinetic profiles, radial electric field, E_r, profiles, and plasma fluctuations have revealed important details of transport barrier physics and the critical importance of E×B velocity shear stabilization of turbulence. Key results from these studies indicate that: (a) changes in E_r occur prior to the H-mode edge barrier formation [7, 8, 9]; (2) there is a distinct reduction in edge density fluctuations and fluctation-driven particle flux coincident with the edge barrier formation [8, 10]; (3) a steep gradient in E_r forms in the region of greatest fluctuation reduction and transport barrier formation [11]; (4) there is a decrease in the radial correlation length of the turbulence at the H-mode transition [12]; (5) there is spatial and temporal correlation between increased E×B velocity shear and reduction in core turbulence and subsequent reduction in core transport [13, 14, 15, 16]. These results are consistent with E×B velocity shear causing reduction in fluctuations leading to transport barrier formation. Further details on the role of E×B velocity shear in reducing transport can be found in the following review articles [17, 18]. In addition, there are recent review articles on experimental and theoretical work on transport barrier formation [19, 20].

More recent studies on transport barriers on DIII-D have focussed on: (1) determining which plasma quantities at the plasma edge are critical for the formation of the edge transport barrier; (2) determining the physics of a quiescent H-mode edge transport barrier which is free from ELMs; (3) combining an internal transport barrier (ITB) with the quiescent edge barrier, and; (4) efforts to control the barriers. For Case 1 above, the experimental approach was to inject frozen deuterium pellets to directly perturb the edge plasma and produce the H-mode edge transport barrier [21]. Measurements of the edge plasma conditions indicated that the attain-

ment of a critical edge temperature (electron or ion) is not required for the H-mode transition. Furthermore, the edge plasma conditions at the pellet-induced H-mode transition have been compared with predictions from models of the H-mode transition [22, 23, 24] and the experimentally determined edge parameters are well below the H-mode threshold values predicted by the theories. These theories, which fit well-developed, mature H-mode conditions, fail at the pellet-induced H-mode transition and so require further development. Also, it has been demonstrated that the pellets can reduce the input power required to produce the H-mode transport barrier by up to 30%. This ability to decrease the power requirement is important for next-step fusion devices in which the available heating power may be marginal for the formation of the H-mode barrier.

The quiescent H-mode plasmas in DIII-D have an H-mode edge transport barrier which is free from ELM activity, but still exhibits good particle control [25, 26]. The increased edge particle transport in these discharges results from a low frequency, continuous MHD oscillation, referred to as the edge harmonic oscillation (EHO), which is located at the base of the edge density pedestal profile at, or just outside, the separatrix [26]. Normally, in standard ELMing H-mode plasmas, the ELMs produce density and impurity control by expelling particles and energy from the confined plasma into the scrape-off layer (SOL) and divertor. The ELMs occur as a result of high edge pressure gradients (associated with the edge transport barrier) combined with edge current density effects [27]. In standard ELM-free discharges, the density and impurity content in the plasma core increases to such a high level that the plasma either disrupts or suffers from high radiative losses so as to revert back to L-mode plasmas. However, the ELMs produce large bursts of heat and particles to the divertor which can result in rapid erosion of the divertor surfaces. Also, giant ELMs can provide seed islands which can trigger core MHD instabilities, such as neoclassical tearing modes. In addition, giant ELMs can penetrate to the plasma core and degrade the internal transport barrier [28]. The quiescent H-mode alleviates these issues associated with the ELMs, whilst maintaining good control of the density and radiated power.

Quiescent ELM-free H-mode barriers have also been observed in the C-Mod tokamak [29, 30, 31], where they are referred to as the "enhanced D_α" (EDA) H-mode. Density and impurity control in the EDA H-mode in C-Mod occurs as a result of a quasi-coherent (QC) oscillation [31, 32] at the plasma edge which drives a large particle flux into the SOL. The EHO in DIII-D and the QC-mode in C-Mod both provide increased particle transport at the plasma edge, but actually have very different characteristics and properties [26]. Also, it should be noted that H-mode barriers

with type II or "grassy" ELMs, which have far lesser perturbative effects than type I ELMs, have been observed in the DIII-D [33], JT-60U [34], and ASDEX Upgrade tokamaks [35]. All these operational regimes are advantageous in that they also have reduced transient heat loads to the divertor surfaces.

Because of the absence of the perturbative effects of giant ELMs in the plasma core, ITBs can be produced and sustained with the quiescent H-mode edge barrier in DIII-D for up to 25 τ_E (i.e., >3.5 s), being limited only by the available neutral beam pulse lengths [36]. These so-called quiescent double barrier (QDB) plasmas have significant performance improvements over. At high input powers, plasma performance of $\beta_N H_{89} \sim 7$ for up to 10 τ_E ($\sim$1.6 s) has been achieved (c.f., $\beta_N H_{89} \sim 4$ for standard ELMing H-mode). Here H_{89} is the confinement enhancement factor relative to ITER89P scaling [37] and, β_N the normalized beta, $= \beta/(I/aB_T)$ [38].

This paper will review the recent advances in edge and internal transport barrier studies on DIII-D. Firstly, details of experimental results from pellet induced H-mode barriers will be presented. This will be followed by sections on the physics of the quiescent H-mode edge barrier and details on the QDB plasmas, including efforts to control the density profiles in QDB plasmas.

2 Pellet-Induced H-Mode Edge Barriers

Edge barriers directly produced by pellet injection in DIII-D exhibit the same features as spontaneously occurring H-mode edge barriers. Figure 1 illustrates the transition to an H-mode plasma as a result of pellet injection. With the neutral beam injected (NBI) power held constant, three frozen deuterium pellets with diameters of 2.7 mm were injected at different times horizontally through a port in the outside vessel wall [i.e., from the low toroidal magnetic field side (LFS) of the plasma]. These LFS pellets were shattered in the guide tube from the injector before entering the vessel in order to mininize the pellet pentration into the plasma so as to produce a density perturbation concentrated near the edge. The neutral beam injected power of 7.3 MW was well below the power required to produced spontaneous (i.e., neutral beam heated) H-mode barriers. The actual H-mode power threshold was greater than 9.2 MW for the operating parameters and plasma configuration in these discharges. The plasma configuration was an unbalanced double-null diverted discharge with the vertical drift of the ions being away from the dominant X-point. Without pellet injection, these plasmas would not transition into H-mode plasmas throughout the beam heated phase (>700 ms). The first pellet in the sequence of 3 broke up into 2 distinct pieces which entered the plasma with a slight time displacement with respect to each other. This can be seen in the trace of the line-averaged density, $\bar{n}_e$, [Fig. 1(b)] and so, subsequently, the edge density perturbation [Fig. 1(d)] was not enough to produce the transition to H-mode. However, the second pellet produced a large enough edge density perturbation to transition into the H-mode. The formation of the edge barrier can be seen from the edge density remaining high and increasing after the second pellet [Fig. 1(d)] even to the point of exceeding the central density about 200 ms later. Both the values of H_{89} and β_N also increase after the second pellet. The third pellet broke up catastrophically in the guide tube and mainly deposited in the scrape-off-layer as can be seen in the divertor photodiode signal at ∼4360 ms [Fig. 1(c)]. Note also the giant ELMs starting at ∼4300 ms [Fig. 1(c)], expelling particles into the SOL and divertor regions. The presence of the giant ELMs indicates the existence of very steep pressure gradients in the edge barrier, which then continue to exist for the duration of the applied neutral beam power. In all aspects, the pellet-induced edge barriers have the same properties as spontaneous, auxiliary heated barriers such as exhibiting hysteresis in power dependence whereby the edge barrier is sustained even as the neutral beam power is decreased below the H-mode power threshold later in the H-mode phase.

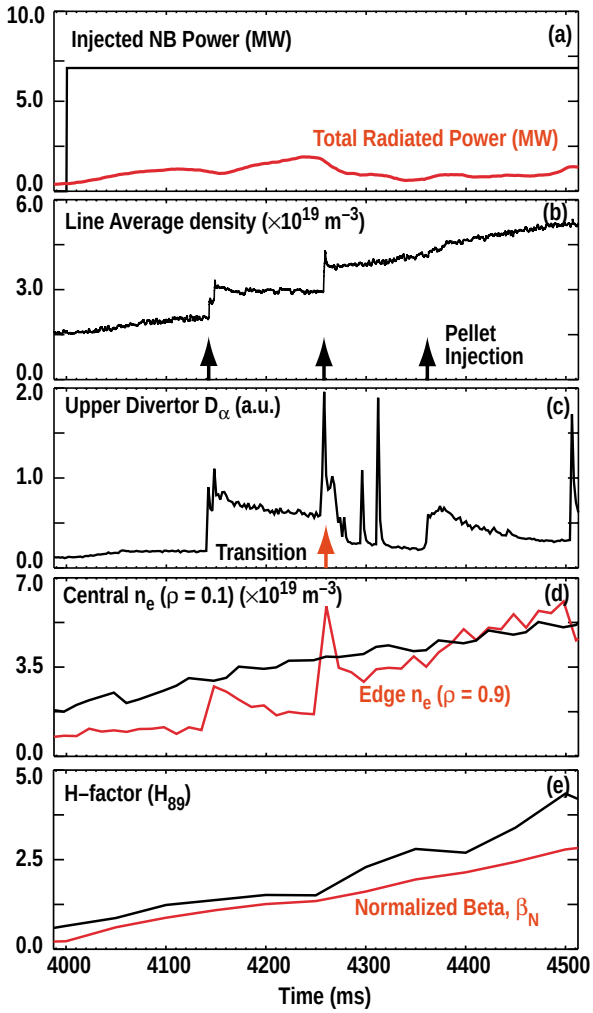

Fig. 1. The time history of a pellet-induced H-mode transition produced by a pellet launched from the LFS of the plasma. (a) Total injected neutral beam power and total radiated power, (b) line-average electron density and times of pellet injection, (c) divertor D_α emission, (d) central and edge electron density, (e) H-factor, H_{89}, and normalized beta, β_N. Plasma current is 1.6 MA and toroidal field is 2.0 T. Notice the large increase in edge electron density on pellet injection, which then remains high and continues to increase as a result of the formation of the edge transport barrier.

The important dynamics of the pellet-induced H-mode edge barrier occur in the region of greatest perturbation by the pellet, i.e., the plasma edge for ρ > 0.9. Figure 2 shows the changes to the profiles of the electron density, n_e, electron temperature, T_e, and ion temperature, T_i, before and after pellet injection for the second pellet shown in Fig. 1. Clearly, the pellet produces substantial increases in the edge density and density gradients just inside the separatrix. At the same time, this produces significant reductions (>50%) in the electron temperature and ion temperature in the same region (ρ > 0.7). The edge barrier is formed during the time of the depressed edge temperatures. After the formation of the edge barrier, both the edge T_e and T_i increase rapidly and within 50 ms exceed the T_e and T_i values prior to pellet injection (i.e., in the L-mode) and pronounced pedestals in the edge T_e and T_i profiles are established indicating the presence of a robust edge transport barrier [21]. The observation of reduced electron and ion temperatures at the time of barrier formation implies that the attainment of a critical edge T_e or T_i value is not necessary for the formation of the H-mode edge barrier. Previous to these experiments, both experimental [39,40] and theoretical studies [23,41,42] had suggested the hypothesis that a critical edge T_e was required for the formation of the H-mode barrier. These studies had based the need for a critical edge temperature on: (a) modeling and fitting to edge local parameters such as n_e and T_e [23,39,41,42]; (b) studies of H-mode transitions triggered by sawtooth heat pulses [43,44]; (c) H-mode power threshold requirements and

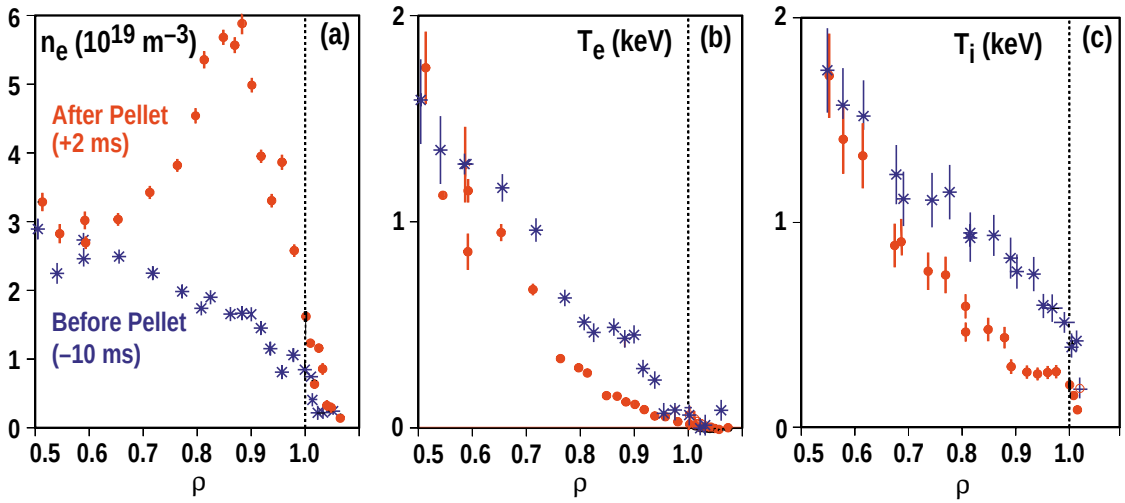

Fig. 2. Electron density and electron and ion temperature profiles at the plasma edge across the pellet-induced H-mode described in Fig. 1. (a) Electron density profile, (b) electron temperature profile, (c) ion temperature profile. The dashed vertical line indicates the position of the separatrix as determined from magnetic equilibrium calculations.

scaling [40]; (d) a critical edge temperature for the stabilization of the drift Alfvén mode [23]. Furthermore, studies of edge temperature behavior are dependent on the exact radial location of the measurement, such as with respect to the position of the separatrix or at a particular point along the edge temperature profile. The ability of the pellet to strongly perturb the edge plasma and lower the edge temperature *everywhere* over a significant region at the plasma edge (for $0.7 < \rho < 1.0$), as can be seen for the T_e and T_i profiles after the pellet in Fig. 2, means that issues relating to uncertainties and ambiguities in the spatial location and absolute value of the temperature measurement become insignificant since the temperature is reduced far below a critical edge temperature over a large region of the plasma. The use of pellet injection, therefore, to directly perturb the edge plasma and significantly lower the edge temperature is the clearest proof that a critical edge temperature alone is not important for the H-mode transition.

Pellet-induced H-mode barriers can be produced at input power levels significantly lower than that required for spontaneous H-mode transitions. Figure 3 shows transition to a H-mode as a result of a single pellet injection from the inside wall of the DIII-D vessel (i.e., from the high field side of the plasma) at a constant NBI power of 4.9 MW. The H-mode transition is indicated by the sharp decrease in the divertor D_α signal [Fig. 3(c)] at the time of pellet injection. In most cases observed so far, there is a short interval (typically ∼20-30 ms) of dithering H-mode (or type III ELMs) after the initial H-mode transition. Once again, [Fig. 3(d,e)] the formation of the edge transport barrier is indicated by the rapid increase in the edge electron density and temperature, which then remain at elevated values as the edge barrier is sustained. Also shown in Fig. 3 is the time evolution of a similar discharge at higher NBI power (∼7.2 MW) which fails to transition to H-mode even in the presence of strong sawtooth activity. The sawteeth can be seen in the sharp increases in the D_α signal and in the edge T_e signal. The sawteeth represent transient heat pulses from the plasma core to the edge and often produce H-mode transitions when the input power level is close to the H-mode threshold power. The absence of sawteeth induced H-mode transitions indicate that these discharges are robust L-mode plasmas even at an input power of 7.2 MW. However, the pellet is able to produce an H-mode edge barrier at even lower NBI power of 4.9 MW, so reducing the power required to produce the H-mode by 2.3 MW or about 30% of the NBI power. This is of great significance for future tokamak devices in which there are large uncertainties in the predicted power required to produce the H-mode transport barrier [45] and in whether the planned input power will be sufficient to produce the barrier. Therefore, any mechanism that can lower the H-mode power threshold requirement, such as pellet injection,

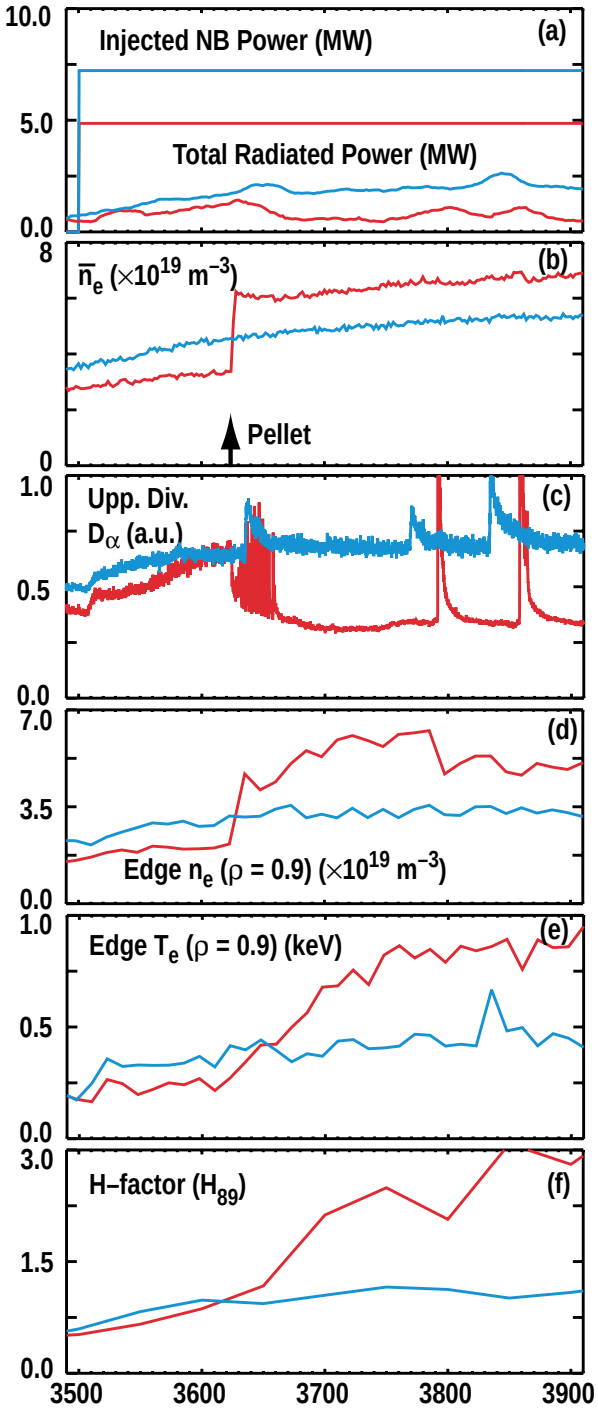

Fig. 3. The time history of a pellet-induced H-mode transition discharge and a reference discharge with no pellet which exhibited no H-mode transition. (a) Total injected beam power and total radiated power, (b) line-average electron density, (c) divertor D_α emission, (d) edge electron density at location ρ = 0.9, (e) edge electron temperature at ρ = 0.9, (f) H-factor, H_{89}. A single pellet is injected at time 3622 ms from the high field side (HFS) of the plasma.

subsequently increases the probability of producing the edge barrier and obtaining the H-mode improved confinement regimes required for high fusion gain.

Pellet injection leads to an increase in the gradient of the radial electric field, E_r, at the plasma edge at the formation of the edge barrier. Figure 4 shows measurements of E_r before and after pellet injection from the inside vessel wall i.e., high magnetic field side of the plasma. The interferometer signal increases dramatically, indicating the large increase in density of pellet injection, and then remains high due to the formation of the edge transport barrier. The D_α signal drops simultaneously indicating the H-mode transition and is followed by a short phase of dithering H-mode, which quickly (<40 ms) turns into an ELM-free H-mode. On pellet injection, the gradient of E_r just inside the separatrix increases substantially and then continues to increase with time and also widens as the edge barrier is firmly established. The values of $|E_r|$ were obtained from charge exchange recombination spectroscopic measurements of the CVI impurity ions. The radial electric field is obtained from the radial force balance equation for any plasma species, i, such that

$$E_r = \frac{\nabla P_i}{n_i Z_i e} + v_\phi B_\theta - v_\theta B_\phi \quad , \tag{1}$$

where n is the species density, P is the pressure, Z is the charge number, e is the electric charge, v_ϕ is the impurity ion toroidal rotation, v_θ is the poloidal rotation, B_ϕ is the toroidal magnetic field and B_θ is the poloidal magnetic field. The greatest changes to the total E_r at the plasma edge are the result of changes to v_ϕ and v_θ of the impurity ion after pellet injection, whereas the core rotation shows less change. The effect on the individual contributions to E_r of ∇P, v_ϕ, and v_θ of the main ions is not determined. However, there are clear increases in the shear in the edge E_r profile for the pellet induced H-mode which is identical in behavior with spontaneous H-mode transitions and is consistent with $E \times B$ velocity stabilization of turbulence leading to the formation of the edge barrier.

The large changes in the edge n_e, T_e, and T_i produced by pellet injection provide a direct means of testing theories on the formation of the H-mode edge barrier. The theories considered [22, 23, 24] postulate certain critical threshold parameters for the H-mode transition determined from the local plasma parameters and their gradients at the plasma edge. These theories have shown agreement with experimental data on nonpellet triggered, spontaneous H-mode transitions in ASDEX Upgrade [23, 42], C-Mod [39, 41] and COMPASS-D [24]. Figure 5 shows the comparisons between experimental results for a H-mode transition produced by a LFS pellet and the threshold parameters postulated by these theories of the H-mode transition. Figure 5(a) is a comparison with the model of Rogers and Drake [22] which is based on 3-D

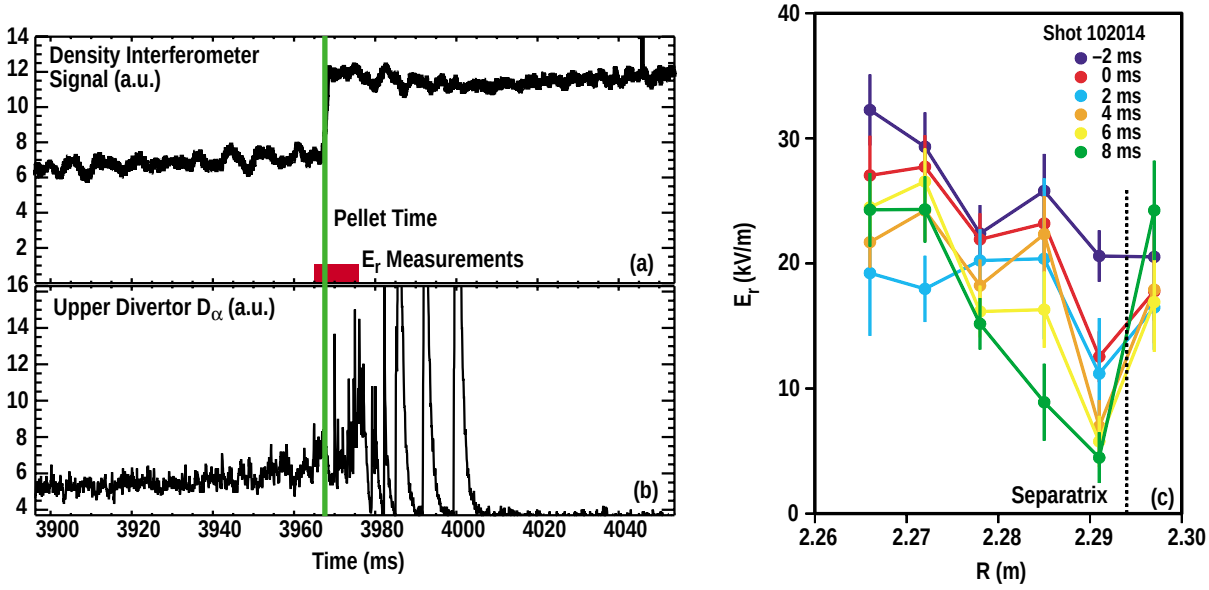

Fig. 4. The time history of a HFS pellet-induced H-mode transition and the radial electric field, E_r, profile at the plasma edge. (a) Density interferometer signal indicating the relative change in the line-average density, (b) upper divertor D_α emission, (c) the E_r profile at the plasma edge. The green solid vertical line in (a) and (b) indicates the time of pellet injection. The red shaded region in (a) indicates the time period for the E_r measurements shown in (c) at a sample time of 2 ms. The dashed vertical line in (c) indicates the position of the separatrix.

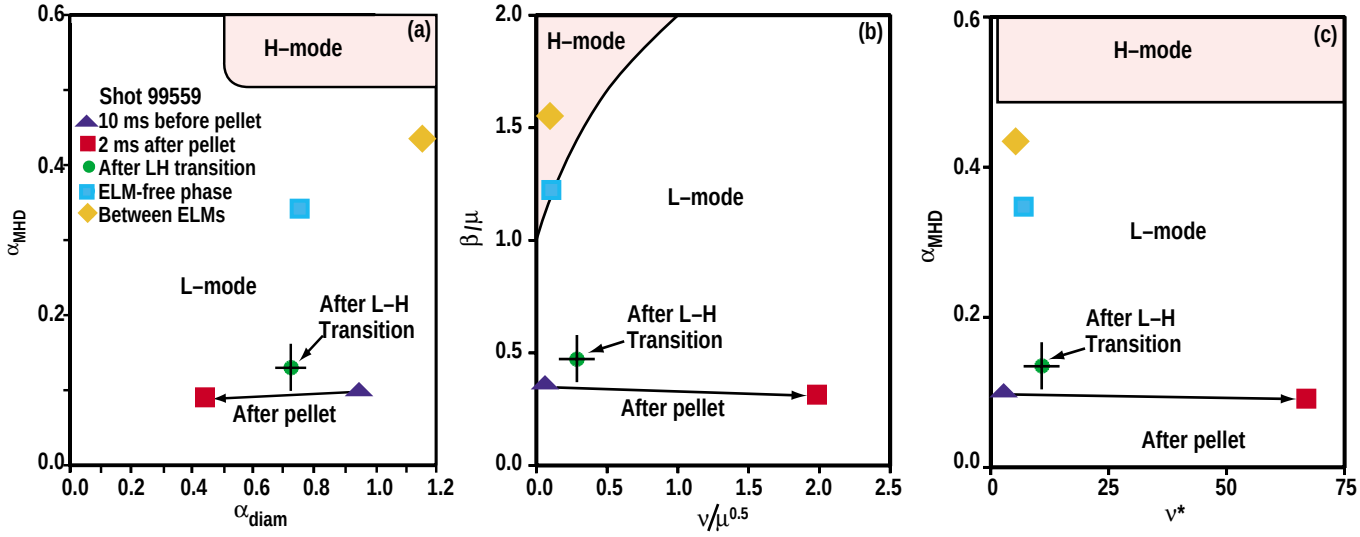

Fig. 5. Comparison of experimental edge local parameters with predictions from three theories of the H-mode transition. (a) Comparison with the model of Rogers and Drake [22], (b) comparison with model of Pogutse *et al.* [23], (c) comparison with nodel of Wilson *et al.* [24].

simulations of the Braginskii equations where the H-mode threshold requirements is parameterized in terms of the edge MHD ballooning parameter α_{MHD} and a diamagnetic parameter α_{DIA}. The model is for a shifted circle magnetic geometry, but the equations have been modified for a closer approximation to the shaped discharges in DIII-D. In their model, transport is suppressed when $\alpha_{MHD} > 0.5$ and $\alpha_{DIA} > 0.5$ in DIII-D. This then defines the parametric region for access to the H-mode (shaded region). The experimental points are evaluated at the location of the maximum edge density gradient and, hence, pressure gradient which gives the highest possible value for α_{MHD} for the various points. The injection of the pellet greatly increases the collisionality and, hence, lowers the α_{DIA} parameters. After the H-mode transition, the increased temperatures lead to increases in the edge pressure (increased α_{MHD}) and to lower edge collisionality (increased α_{DIA}). Also shown are the experimental points well into the H-mode and just before a giant ELM. These conditions are in closer agreement to the model requirements, but represent well established H-mode values by which time the edge pressure gradients have increased substantially as a result of the previously formed transport barriers.

In another model of the H-mode transition by Pogutse *et al.*, [23] an increased plasma pressure leads to the Alfvén waves mixing with the electron drift waves and stabilizing the long wavelength turbulence. Their Alfvén drift model predicts that turbulent transport is suppressed when $\beta_N > 1 + \nu_N^{2/3}$, where β_N and ν_N are the edge normalized beta and normalized collision frequency, respectively. This inequality is satisfied for the shaded region in Fig. 5(b) and represents the requirements for the H-mode transition. The experimental values for β_N and ν_N are well below the model predictions for all points up to and through the H-mode transition.

In another model of the H-mode transition, unstable peeling modes at low edge collisionality are invoked by Wilson *et al.* [24] to explain the increased difficulty in obtaining H-mode transitions at low edge collisionality in the COMPASS-D tokamak. At higher edge collisionality ($v^* > 1$), the peeling mode can be stabilized by increasing the edge pressure gradient, i.e., $\alpha_{MHD} > 0.5$ and $v^* > 1$. This parameter space for reduced transport and improved confinement is shown in Fig. 5(c). Once again, the experimental edge pressure gradient at the H-mode transition is far below the theoretical predictions. The theories exhibit near agreement with the experimental data later into the H-mode implying that the theories appear to be more applicable to well established H-mode since the edge pressure gradients have naturally increased significantly due to the improved edge confinement. However, they are clearly inadequate in describing the conditions at the H-mode transition itself.

3 Quiescent H-Mode Edge Barrier

The key requirements for producing the quiescent H-mode barrier in DIII-D are: (a) neutral beam injection opposite to the direction of the plasma current (counter-NBI); (b) edge cryopumping to maintain a low edge plasma density and remove particles from the SOL; (c) a large gap (>10 cm) between the plasma edge and the outside vessel wall (i.e., at LFS of the plasma). Figure 6 shows the time evolution of several important features of quiescent H-mode plasmas. The quiescent phase appears spontaneously after a short period of ELMing H-mode and is then sustained for about 3.5 s or 25 τ_E, and lasts for the duration of the applied neutral beams and the plasma current. During this time, the line-averaged density and radiated power are maintained at near constant levels indicating that density control is in effect similar to that in standard ELMing H-modes, but in this case without the presence of ELMs. Note that in a standard ELM-free H-mode, the electron density and radiative power would continue to increase until radiative collapse terminates the H-mode phase. The quiescent H-mode phase is also associated with a profound change in the magnetic probe signal, from a sporadic bursting nature to a continuous, gradually

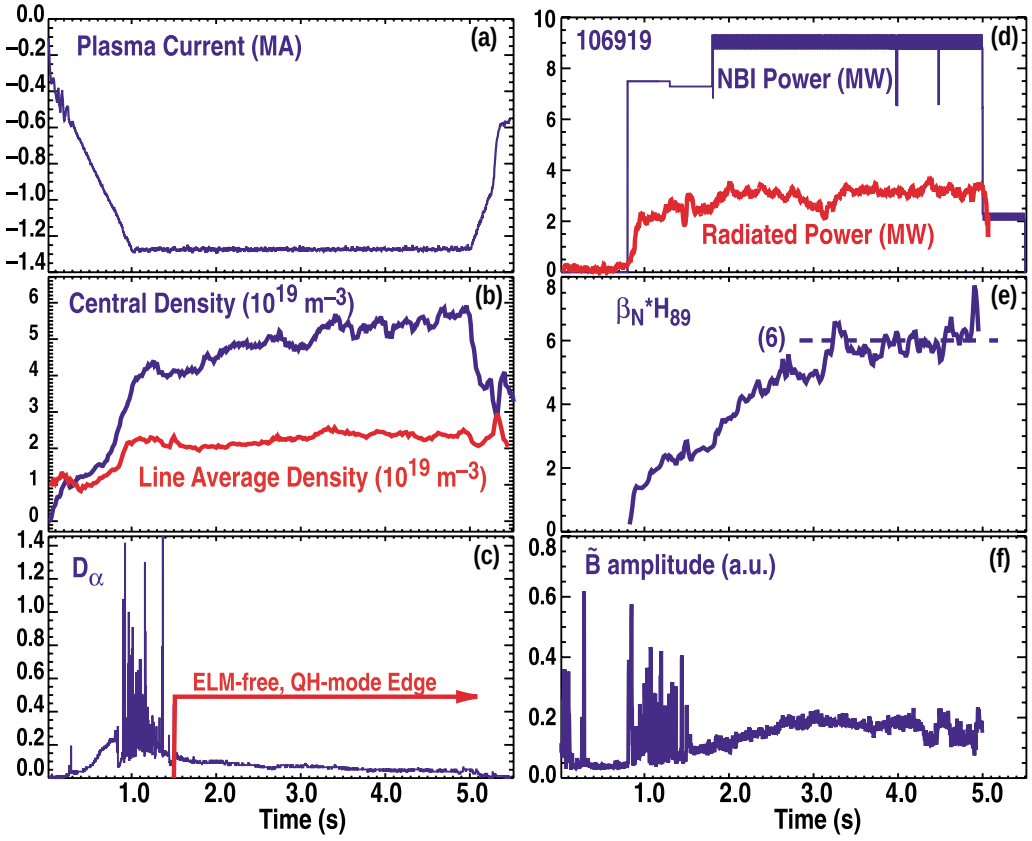

Fig. 6. The time history of a quiescent H-mode discharge. (a) Plasma current, (b) total injected beam power and total radiated power, (c) divertor D_α emission, (d) central electron density and line-average density, (e) product of H_{89} and β_N, (f) $\tilde{B}_\theta$ from magnetic probe. The toroidal field is 2.0 T.

varying signal [Fig. 6(f)]. This continuous signal represents the emergence of a low to moderate n ($n = 1 - 10$) MHD oscillation, known as the edge harmonic oscillation, which is responsible for the increased edge particle transport. For quiescent H-mode operation,the edge density must be kept low (i.e., typically 1-2$\times 10^{19}\,\mathrm{m}^{-3}$ at the top of the H-mode pedestal, although $4\times 10^{19}\,\mathrm{m}^{-3}$ has been observed) which stresses the importance of the cryopump, since any increase in the edge density, e.g., due to pellet injection or gas puffing, results in a reversion to ELMing H-mode. This low density operation is in contrast to the EDA H-modes in C-Mod, which typically have a threshold in the line-averaged densities of $1.2\times 10^{20}\,\mathrm{m}^{-3}$, above which the EDA H-mode is obtained and below which a standard ELM-free H-mode is obtained [31]. However, it should be noted that this threshold density is quite low for C-Mod operation, being close to the low density limit for H-mode in C-Mod and being only 15% of the Greenwald density limit. This latter value is similar to the edge pedestal density for quiescent H-mode in DIII-D, which is between 10%-20% of the Greenwald density [26].

The quiescent H-mode edge barrier exhibits the same or higher temperature and pressure gradients as observed in the ELMing H-mode barrier. This is shown in Fig. 7, which compares the edge profiles during the ELMing phase and the quiescent phase of the discharge shown in Fig. 6. The edge electron density is slightly lower in the quiescent phase indicating the increased edge particle transport due to the EHO. However, the energy transport barrier is maintained as exhibited by the higher edge temperatures and pressures and their respective gradients. In particular, the edge ion temperature and ion temperature gradient is significantly higher in the quiescent H-mode barrier. High ion temperatures are observed in the SOL during both the ELMing and quiescent phases. This is probably due to the relatively high number of fast ions in the SOL resulting from the use of counter-NBI. The quiescent H-mode barrier is clearly a robust edge transport barrier. Furthermore, the barrier conditions are maintained throughout the quiescent phase as shown by the lack of change in the maximum edge electron pressure gradient in the transition from the ELMing phase [Fig. 7(b)].

In nearly all cases the quiescent H-mode is associated with the EHO, apart from one case in which the density control occurs as a result of a core tearing mode. Understanding the quiescent H-mode barrier then requires determining the physics of the EHO, particularly with regard to counter-NBI operation. The EHO manifests itself through magnetic, density and temperature fluctuations at the plasma edge, which are highly coherent with respect to each other. Magnetic probe data indicates

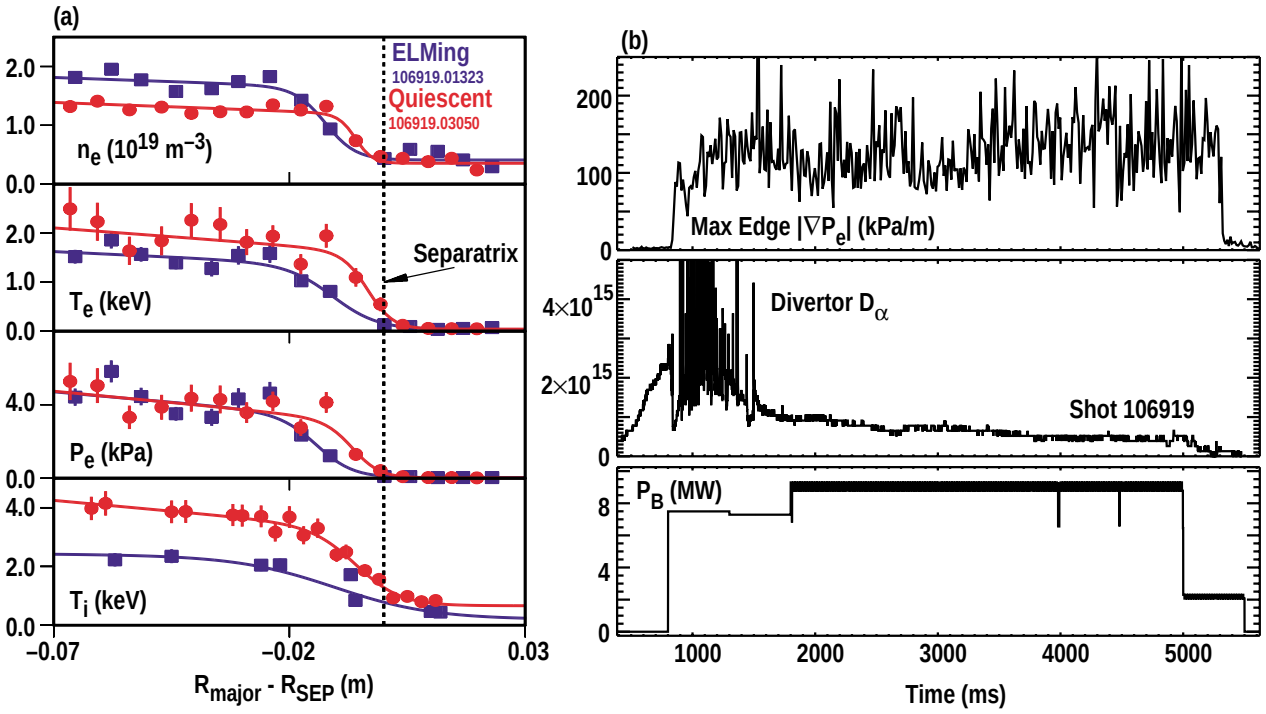

Fig. 7. Edge profiles for the quiescent and ELMing phases of the discharge described in Fig. 6 and also time history of the maximum edge electron pressure gradient. (a) Edge profiles of electron density, temperature and pressure and of the ion temperature, (b) the maximum edge electron pressure gradient, divertor D_α emission and total injected beam power. The dashed vertical line in (a) signifies the location of the separatrix. The maximum edge electron pressure gradient is determined from a hyperbolic target fit to the electron pressure profiles measured by Thomson scattering.

a mixture of frequencies associated with toroidal mode numbers (i.e., n=1, 2, 3, etc.) representative of the fundamental frequency and its harmonics with typical frequencies of 6-10 kHz for the n=1. This multiharmonic activity can be seen in Fig. 8, which also indicates that the amplitude and harnonic distribution of the mix of frequencies can change spontaneously. However, these changes do not affect the edge pressure gradient and both particle control and the energy transport barrier are maintained throughout these changes. Measurements of the particle flux from the ion saturation current to Langmuir probes in the divertor in the region of the SOL show the same harmonic frequency behavior as the magnetic probe data [26]. This indicates that the EHO is responsible for the particle flux into the SOL and divertor. Furthermore, the quiescent H-mode is lost when the EHO disappears at which point the discharge reverts back to an ELMing H-mode plasma after a short period of standard ELM-free plasma.

In the case of C-Mod, the quasi-coherent mode, which is only observed when the discharge is in the EDA H-mode, has been determined to exist in the steep density gradient region at the plasma edge from fluctuation measurements from a fast-scanning Langmuir probe. Typical frequencies of the QC-mode, which appears to be responsible for the enhanced edge particle transport in the EDA H-mode, are in the range 100-150 kHz which

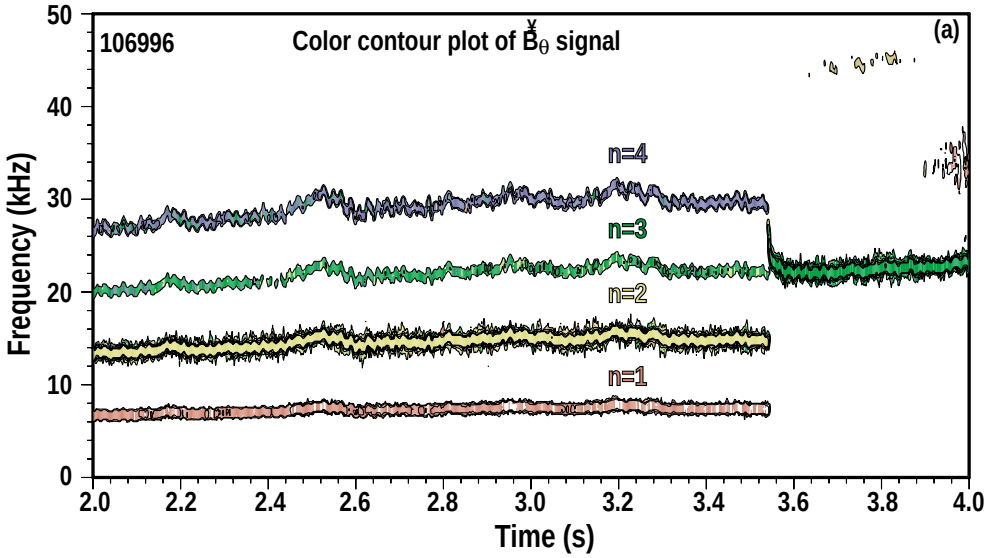

Fig. 8. Time history of the mix of toroidal mode number *n* associated with the EHO (from magnetic probe measurements). Notice that the EHO exhibits a mix of *n*=1, 2, 3, and 4 with the dominant mode being *n*=2 and then spontaneously changes to *n*=3 dominant with the loss of the other modes.

is significantly higher than the 6-10 kHz (*n*=1) for the EHO in DIII-D. The QC-mode is only observed on the Langmuir probe when the tip is within a few millimeters of the last closed flux surface (LCFS) of the plasma [32]. Another major difference between the EHO in DIII-D and the QC-mode in C-Mod is in the poloidal wavelength which is of the order 100 cm in DIII-D and about 1 cm in C-Mod.

The reason for the onset of the EHO is, as yet, unknown. It is observed most frequently in counter-NBI discharges, although it has appeared in co-NBI discharges, but always in the presence of giant ELMs in the latter case. As yet, quiescent H-mode barriers have only been obtained with counter-NBI. The reason for the disappearance of the ELMs has not been determined. Certainly, the presence of the EHO is not the reason for the absence of the ELMs since both have been observed together in co-NBI discharges. The hypothesis that the EHO is a saturated MHD precursor to an ELM is not consistent with observations of the temporal behavior of the EHO and ELM activity [26]. One large difference between quiescent H-mode and the ELMing H-mode phase is the much deeper extent of the E_r well at the plasma edge in the quiescent phase, as shown in Fig. 9(a). Similarly, the E_r well in the quiescent H-mode is also much deeper than the E_r structure in the ELM-free phase of a co-NBI discharge [Fig. 9(b)]. As yet, this is an observation and no theory presently exists for the influence of shear in E_r on the stabilization of ELMs.

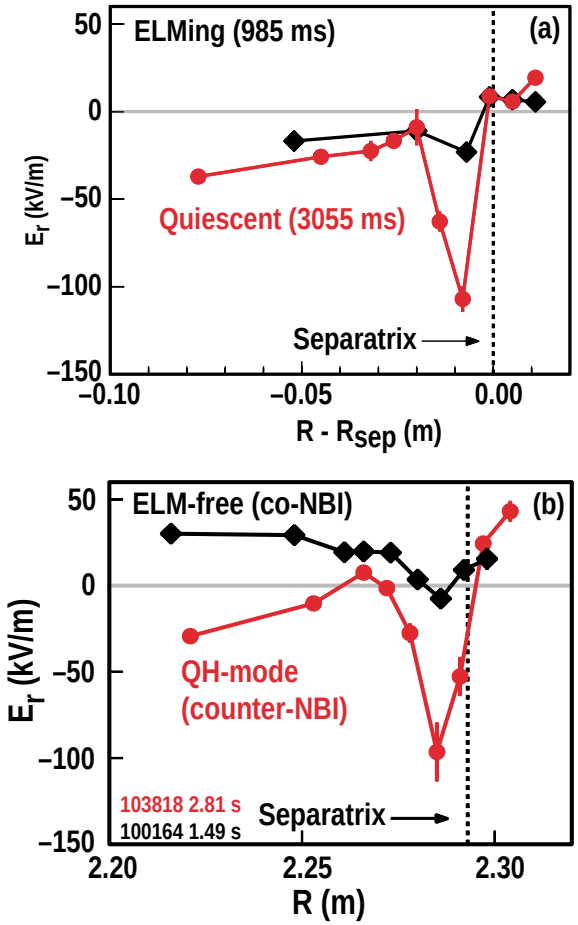

Fig. 9. Edge profiles of the radial electric field, E_r, in quiescent H-mode and standard ELM-free and ELMing H-mode discharges. (a) Comparison of the edge E_r, profile during the quiescent and ELMing phases of the same H-mode discharge shown in Fig. 6. (b) Comparison of the edge E_r, in a counter-injected quiescent H-mode discharge (103818) and the ELM-free H-mode phase of a co-injected discharge (100164). The E_r, profiles are determined by charge exchange spectroscopy of the CVI impurity ion.

4 Quiescent Double Barrier Plasmas

The quiescent double barrier plasma in DIII-D is the result of the co-existence of an internal transport barrier with the quiescent H-mode edge barrier and, as is the nature of the quiescent H-mode, has so far only been observed in counter-NBI discharges. The two transport barriers are able to co-exist because of the absence of the core perturbative effects of giant ELMs, normally prevalent in standard ELMing H-mode discharges. Figure 10 illustrates the spatial features of the QDB density and temperature profiles, indicating clear simultaneous transport barriers in the plasma core and edge in sharp contrast to the poor confinement exhibited by the L-mode profiles. The effects of the two barriers is additive in the sense that the elevated temperatures in the edge barrier lead to increased temperatures in the plasma core compared to standard ITBs with an L-mode edge. Increasing the NBI heating power normally results in strengthening the ITB with little change to the edge barrier. The combination of the two barriers results in high performance plasmas with $\beta_N H_{89} \sim 7$ sustained for up to 10 τ_E and only being limited by the length of the neutral beam pulse duration. The separation of the core and edge barriers in QDB plasmas appears to be related to the location where the $E \times B$ shearing rate is zero valued, which results from a local maximum in the E_r profile near the plasma edge [25]. Subsequently, a region of high transport due to decreased $E \times B$ velocity shear stabilization would inhibit the coalescence of the two barriers.

The ITB in QDB plasmas is maintained without complete stabilization of the turbulence as indicated by the large amplitude of the broadband turbulence measured by FIR scattering [46]. However, the transport is calculated to be quite small in the plasma core, despite the large turbulence amplitude. Instead, the reason for the reduced core transport is the reduced step size for transport in the plasma core as indicated by correlation reflectometry measurements which show a significant decrease in the turbulence correlation lengths in the core of QDB plasmas [25]. In fact, the correlation length remains fairly constant (1-2ρ_s, where ρ_s is the ion gyroradius) over the plasma radius instead of tracking the ion gyroradius as observed in L-mode plasmas [47]. This indicates that the relative (or percentage) decrease in the correlation length is greater towards the plasma core and explains the reduced core transport even in the presence of finite turbulence. Simulations of QDB plasmas using the UCAN global gyrokinetic [48] code also predict a significant reduction of the correlation length of turbulence in the plasma core.

The peaked density profiles in QDB plasmas [Fig. 10(d)] are a result of the low edge density, along with centrally peaked neutral beam particle fueling, low core transport and accumulation of impurities. The peaked density profiles then lead to further increase in the influx of high-Z impurities (nickel and copper). Although core nickel concentrations can be as high as 0.3% [49], the radiative power is low since nickel and copper, at the electron temperatures in QDB plasmas (~5 keV), are dominantly in the helium-like ionization state which have low radiation efficiencies. However, this leads to a reduction in the neutron flux as a result of dilution of the main fuel ions. The carbon fraction across the plasma radius remains fairly at constant with time at about 4%. A total Z_{eff} in the plasma core of 6.5 in QDB plasmas has been observed [49].

Control of the electron density profile to reduce its peakedness then becomes important in order to reduce the impurity accumulation and the central Z_{eff} so as to increase the neutron production rates. One approach that has been effective in reducing the central density and the profile peakedness in QDB plasmas is the application of central electron cyclotron heating (ECH). Figure 11 shows the effect of applying about 2 MW of central ECH power (at ρ = 0.12) on the electron density profile. Figure 11(a) shows that the central electron density decreases on application of the ECH and continues to decrease until the ECH power is reduced in a stepwise manner, at which point the central density begins

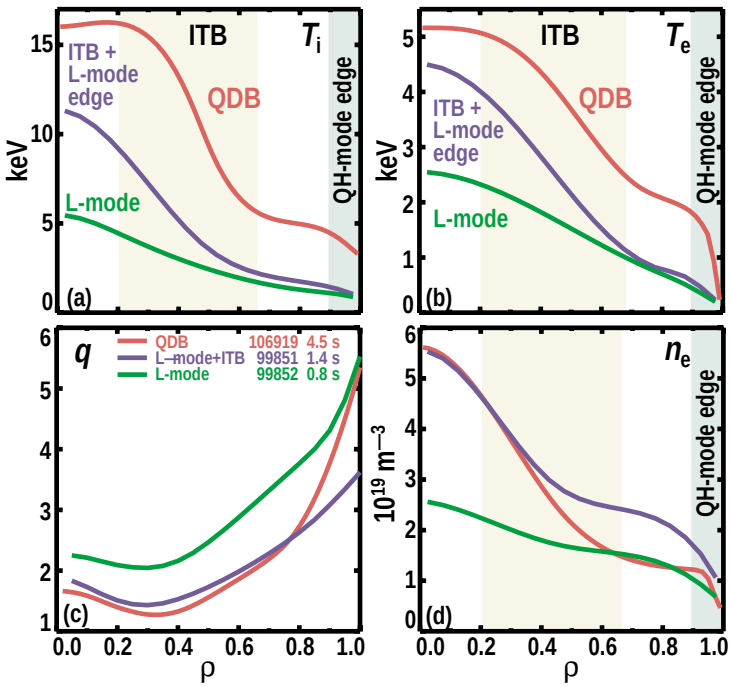

Fig. 10. Comparison of radial profiles for a QDB discharge, a L-mode discharge and a discharge with ITB and L-mode plasma edge. (a) Ion temperature profiles, (b) electron temperature profiles, (c) safety factor, q, profiles, (d) electron density profile. The shaded region indicates the relative locations of the quiescent edge barrier and the internal transport barrier.

to increase and finally reverts back to the pre-ECH value by the end of the ECH pulse. There is clear correlation between the value of central electron density and the amount of applied ECH power. Figure 11(b) shows a clear decrease in both the central density and the peakedness of the profiles with ECH. The peaking ratio, $n_e(0)/\bar{n}_e$, decreases from 2.7 to 1.7 after 400 ms of ECH. The decrease in the central density is accompanied by a slight increase in the edge density as a result of the redistribution of particles from the core to the edge. This leads to the onset of sporadic ELM activity, although discharges have been obtained which are ELM-free during ECH. The onset of ELM activity may be related to the degree by which the edge density increases during the ECH since this behavior is similar to gas puffing or pellet injection which leads to ELM activity as a result of increased edge density. After an initial slight decrease, the line-averaged density is observed to increase very gradually over time. This is a result of both the weakening of the EHO and the onset of the ELMs. Preliminary results from the multi-ionization state transport code (MIST) [50] using the measured electron density and temperature profiles and the measured VUV indicate that the central density of Ni brightness of Ni lines also decreases [Fig. 11(c)] with the reduction in the central electron density and the profile peakedness. Therefore, control of the electron density profile has led in turn to control of the high-Z impurities in these plasmas. However, for effective steady-state, high performance operations, it is real time control of the profiles [e.g., $n_e(r)$, $T_e(r)$, $T_i(r)$, $q(r)$, etc.] that is required. Efforts are underway at DIII-D to implement real-time control of profiles using feedback from diagnostic systems measuring the profiles onto actuators (e.g., ECH, ECCD, NBI, pellet injection, gas puff, etc.) that can change the profiles.

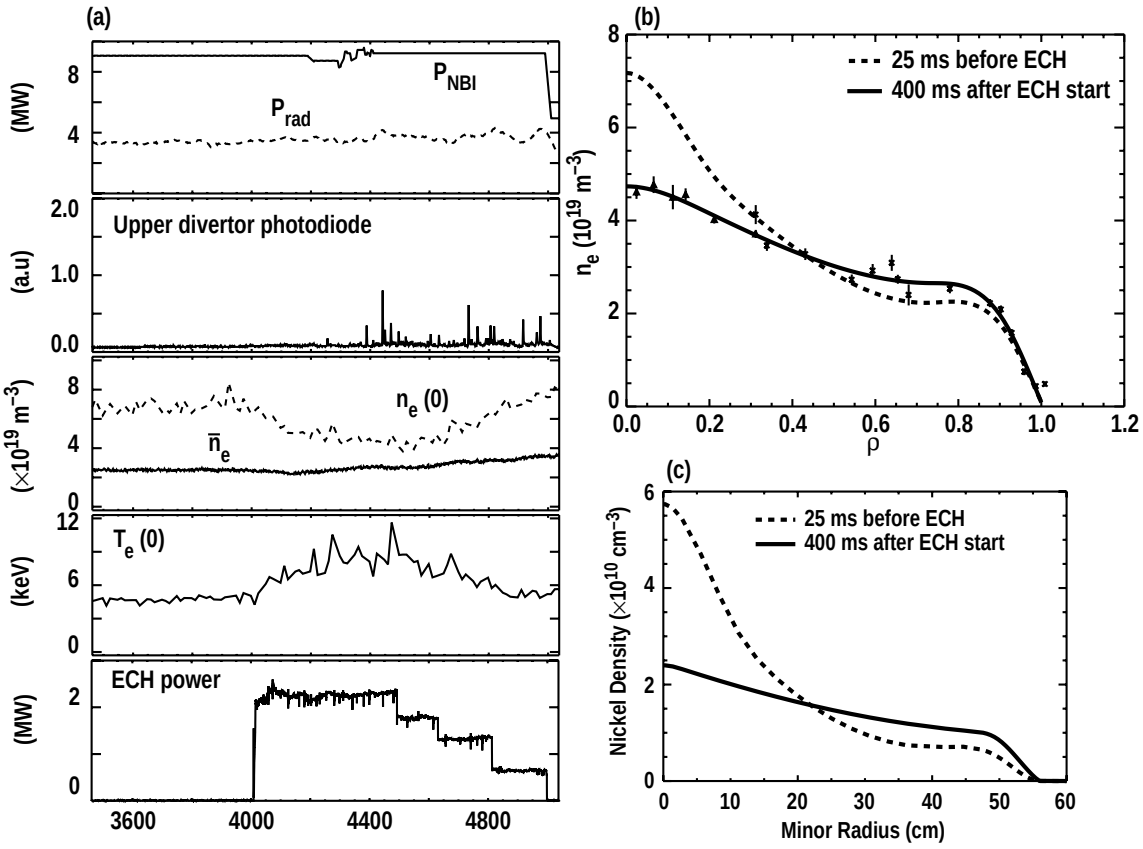

Fig. 11. (a) Time histories of various quantities indicating the reduction in central electron density by on-axis ECH. (b) Profiles of the electron density before and after application of ECH. (c) Profiles of the nickel impurity concentration before and after ECH.

5 Summary

Results from experiments on the DIII-D tokamak have revealed many important details on transport barriers at the plasma edge and in the plasma core. A large body of work has revealed that stabilization of turbulence by $E \times B$ velocity shear can explain the formation of transport barriers located anywhere from the plasma edge to the plasma core. More recent experiments on DIII-D have revealed details on: (a) the formation of the H-mode edge barrier directly by pellet injection; (b) the formation of a quiescent H-mode edge barrier which is ELM-free, but which still exhibits density control; (c) the formation of the quiescent double barrier which combines an internal transport barrier with the quiescent edge barrier.

Pellet injection leads to the formation of a large shear in the edge E_r profile at the formation of the H-mode barrier, similar to observations of changes to the E_r profile for spontaneously occurring H-mode barriers, which result from heating the plasma edge. The large increase in the edge electron density from pellet injection leads to a large decrease in the edge electron and ion temperatures, but which still results in the formation of the H-mode barrier. This indicates that the attainment of a critical edge temperature (electron or ion) is not required for the formation of the edge H-mode transport barrier. The pellet is also able to reduce (by up to 30%) the power threshold required to produce the H-mode barrier, which appears to be favored by the production of a large density gradient by the pellet at the plasma edge. The large change in the edge electron density and temperature and ion temperature produced by pellet injection provide a direct means of testing theories on the formation of the H-mode barrier. The experimentally determined edge plasma parameters at the formation of the pellet-induced H-mode barrier are well below the predictions of several theories on the H-mode transition so providing valuable data for improving these theories.

Quiescent H-mode edge barriers are free from ELM activity and, hence, have no pulsed heat loads to the divertor. The QH-mode edge barrier requires counter-NBI together with strong cryopumping and a large gap between the plasma edge and the vessel wall at the low field side of the plasma. Density and radiative power control in these plasmas is the result of enhanced edge particle transport due to the spontaneously occurring EHO. Despite the enhanced particle transport, the EHO does not affect the energy transport in the quiescent edge barrier since steep edge gradients in T_e, T_i, and P_e are produced, similar (or greater) in magnitude to edge gradients in standard ELMing H-mode plasmas. The reason for the spontaneous appearance of the EHO activity is, as yet, unknown. The reason for the disappearance of the ELMs

also needs to be determined, although it is not due to the presence of the EHO itself. Very large gradients in the edge E_r are observed in the quiescent H-mode barrier compared to the ELMing edge barrier in the same discharge and the influence of E_r shear on ELM stabilization needs to be assessed.

The absence of the perturbative effects of giant ELMs have resulted in discharges with an internal transport barrier combined with the QH-mode edge barrier. These QDB plasmas have higher plasma performance than standard ELMing H-mode plasmas, primarily as a result of the improved confinement in the plasma core. The central electron and impurity densities and the electron density peakedness in QDB plasmas can be reduced on application of on-axis ECH. The cause of the central density reduction by ECH needs to be determined and will be the subject of further studies.

The above studies of transport barriers on DIII-D have favorable consequences for future fusion devices. The use of pellet injection increases the probability of obtaining the H-mode edge barrier by lowering the power threshold for barrier formation. The quiescent H-mode barrier eliminates the high pulsed heat loads to the divertor, dramatically reducing erosion of the divertor surfaces. The quiescent double barrier regime provides for higher fusion performance than standard ELMing H-mode discharges so increasing the margin in confinement required for attaining the target Q in these devices.

References

[1] Biglari, H., *et al.*, Phys. Fluids **B 2**, 1 (1990).

[2] Shaing, K.C., *et al.*, Phys. Fluids **B 2**, 1492 (1990).

[3] Waltz, R.E., *et al.*, Phys. Plasmas **2**, 2408 (1995).

[4] Wang, X.H., *et al.*, Phys. Fluids **B 4**, 2402 (1992).

[5] Beer, M.A., *et al.*, Phys. Plasmas **4**, 1792 (1997).

[6] Drake, D.F., *et al.*, Phys. Rev. Lett. **77**, 494 (1996).

[7] Burrell, K.H., *et al.*, in *Proceedings of the Fifteenth International Conference on Plasma Physics and Controlled Fusion*, Vol. 1 (International Atomic Energy Agency, Vienna, 1995) p. 221.

[8] Moyer, R.A., *et al.*, Phys. Plasmas **2**, 2397 (1995).

[9] Burrell, K.H., *et al.*, Rev. Sci. Instrum. **72**, 906 (2001).

[10] Moyer, R.A., *et al.*, Plasma Phys. and Control. Fusion **41**, 243 (1999).

[11] Gohil, P., *et al.*, Nucl. Fusion **34**, 1057 (1994).

[12] Coda, S., *et al.*, Phys. Lett. A **273**, 125 (2000).

[13] Rettig, C.L., *et al.*, Phys. Plasmas **5**, 1727 (1998).

[14] Burrell, K.H., *et al.*, Plasma Phys. and Control. Fusion **40**, 1589 (1998).

[15] Doyle, E.J., *et al.*, in *Proceedings of the Sixteenth International Fusion Energy Conference*, Montreal, 1996 (International Atomic Energy Agency, Vienna, 1997) Vol. I, p. 547.

[16] Schissel, D.P., *et al.*, in *Proceedings of the Sixteenth International Fusion Energy Conference*, Montreal, 1996 (International Atomic Energy Agency, Vienna, 1997) Vol. I, p. 463.

[17] Burrell, K.H., *et al.*, Phys. Plasmas **4**, 1499 (1997).

[18] Burrell, K.H., *et al.*, Phys. Plasmas **6**, 4418 (1999).

[19] Gohil, P., *et al.*, Plasma Phys. and Control. Fusion **44**, A37 (2002).

[20] Hahm, T.S., *et al.*, Plasma Phys. and Control. Fusion **44**, A87 (2002).

[21] Gohil, P., *et al.*, Phys. Rev. Lett. **86**, 644 (2001).

[22] Rogers, B.N., and J.F. Drake, Phys. Rev. Lett. **81**, 4396 (1998).

[23] Pogutse, O., *et al.*, in *Proceedings of the Twenty-Fourth European Conference on Controlled Fusion and Plasma Physics*, Berchtesgaden, 1997 (European Physical Society) Vol. 21A, p. 1041.

[24] Wilson, H.R., *et al.*, Phys. Plasmas **6**, 1925 (1999).

[25] Burrell, K.H., *et al.*, Phys. Plasmas **8**, 2153 (2001).

[26] Burrell, K.H., *et al.*, Plasma Phys. and Control. Fusion **44**, A253 (2002).

[27] Wilson, H.R., *et al.*, Phys. Plasmas **9**, 1277 (2002).

[28] Sips, A.C.C, *et al.*, Nucl. Fusion **41**, 1559 (2001).

[29] Takase, Y., *et al.*, in *Proceedings of the Sixteenth International Fusion Energy Conference*, Montreal, 1996 (International Atomic Energy Agency, Vienna, 1997) Vol. I, p. 475.

[30] Greenwald, M., *et al.*, Phys. Plasmas **6**, 1943 (1999).

[31] Hubbard, A.E., *et al.*, Phys. Plasmas **8**, 2033 (2001).

[32] Snipes, J.A., *et al.*, Plasma Phys. and Control. Fusion **43**, L23 (2001).

[33] Ozeki, T., *et al.*, Nucl. Fusion **30**, 1425 (1990).

[34] Kamada, Y., *et al.*, Plasma Phys. and Control. Fusion **42**, A247 (2000).

[35] Stober, J., *et al.*, Plasma Phys. and Control. Fusion **42**, A211 (2000).

[36] Greenfield, C.M., *et al.*, Phys. Rev. Lett. **86**, 4544 (2001).

[37] Yushmanov, P., *et al.*, Nucl. Fusion **30**, 1999 (1990).

[38] Taylor, T.S., *et al.*, Plasma Phys. and Control. Fusion **36**, B229 (1994).

[39] Hubbard, A., *et al.*, Plasma Phys. and Control. Fusion **40**, 689 (1998).

[40] Ryter, F., *et al.*, Plasma Phys. and Control. Fusion **40**, 725 (1998).

[41] Janeschitz, G., *et al.*, in *Proceedings of the Twenty-Fourth European Conference on Controlled Fusion and Plasma Physics*, Berchtesgaden, 1997 (European Physical Society) Vol. 21A, p. 993.

[42] Igitkhanov, Y., *et al.*, Plasma Phys. and Control. Fusion **40**, 1585 (1998).

[43] Wagner, F., *et al.*, Phys. Rev. Lett. **53**, 1453 (1984).

[44] ASDEX Team, Nucl. Fusion **29**, 1959 (1989).

[45] ITER Physics Basis Document, Nucl. Fusion **39**, 2137 (1999).

[46] Greenfield, C.M., *et al.*, Plasma Phys. and Control. Fusion **44**, A123 (2002).

[47] Rhodes, T.L., *et al.*, Phys. Plasmas **9**, 2141 (2002).

[48] Sydora, R.D., *et al.*, Plasma Phys. and Control. Fusion **38**, A281 (1996).

[49] West, W.P., *et al.*, Phys. Plasmas **9**, 19701 (2002).

[50] Hulse, R.A., Nucl. Technol./Fusion **3**, 259 (1983).

Acknowledgment

This is a report of work supported by the U.S. Department of Energy under Contract Nos. DE-AC03-99ER54463, DE-AC05-00OR22725, W-7405-NG-48, DE-FG03-01ER54615, DE-FG02-92ER54141, DE-FG03-95ER54294, and DE-AC04-94AL85000.